A Fast Impedance Measurement Method for Lithium-ion Battery Using Power Spectrum Property

Peng, Jichang; Meng, Jinhao ; Du, Xinghao; Cai, Lei; Stroe, Daniel-Ioan

Published in:
I E E E Transactions on Industrial Informatics

DOI (link to publication from Publisher):
10.1109/TII.2022.3217474

Publication date:
2022

Document Version
Accepted author manuscript, peer reviewed version

A Fast Impedance Measurement Method for Lithium-ion Battery Using Power Spectrum Property

Jichang Peng, Jinhao Meng, *IEEE Member*, Xinghao Du, Lei Cai and Daniel-Ioan Stroe, *IEEE Member*

***Abstract*—Electrochemical Impedance Spectroscopy (EIS) can provide fruitful information for Lithium-ion (Li-ion) battery modelling and diagnosis, yet EIS measurement is time-consuming with low-frequency signal injection. By stacking a group of broadband signals, Pseudo Random Sequence (PRS) makes it possible to obtain the battery EIS in a few seconds at the expense of measurement accuracy and Signal-to-Noise Ratio (SNR). Thus, this paper focuses on developing a highly effective signal processing procedure to extract useful information from the PRS for accurate EIS measurement. To enhance the ability of the data cleaning procedure, a three-dimensional cloud is firstly reconstructed for each impedance by integrating its Power Spectrum (PS). The impedance with lower PS can be easily removed through a statistical based multiple selection mechanism, which enables the extraction of the EIS without altering the original measurement. Experimental results on a 3000mAh Li-ion battery prove the effectiveness of the proposed method.**

***Index Terms*—Lithium-ion battery, Pseudo random sequence, Power spectrum, Statistical selection, Electrochemical impedance spectroscopy.**

I. Introduction

THANKS to their superior properties in comparison to other technologies, Lithium-ion (Li-ion) batteries have been a dominant component for energy storage applications such as Electric Vehicles (EV) and consumer electronics. Considering that there have been nearly 6.74 million units for global EV sales in 2021 [1], advanced technologies to help manage the usage of Li-ion batteries are of great importance in every aspect.

The battery can transfer the chemical energy to electrical energy utilizing the electrochemical potential between the two electrodes. Unfortunately, due to various aging mechanisms, the performance of the batteries is incrementally decreasing being visible as capacity decreases and resistance increases (i.e., power fade). The lithium metal (-3.04V, 3850mAh/g) has a higher reduction potential and gravimetric capacities than the others materials like sodium (-2.71V, 1165mAh/g), magnesium (-2.37V, 2046mAh/g) and aluminum (-1.66V, 2978mAh/g) [2]. Thus, the Li-ion battery has the great merits of high energy/power density, but its voltage is still limited to less than 5V which indicates one single cell can not fulfil the requirement of a high power load as EVs. Normally, a group of cells will be connected in series or parallel to implement such a task. In this thread, Battery Management System (BMS) plays a key role in the electric, thermal and lifespan management of each cell, and the battery SOX (state of charge, state of health, state of power, state of function, *etc.*) is the critical indicators for a BMS functionality. Therefore, there is an urgent need to diagnose and prognose the status of the Li-ion battery, and to understand its electrochemical reactions mechanism for a specific battery-based application.

Electrochemical Impedance Spectroscopy (EIS) can provide fruitful information for the electrode kinetics, which has a great potential to be used for the Li-ion battery SOX estimation [3]–[5], the degradation pattern identification [6], [7], internal temperature estimation [8], [9], and safety monitoring [10], [11]. For example, over 20,000 EIS measurements from 45mAh Li-ion cells can accurately reflect the battery degradation pattern by Gaussian process regression in [6]. The distribution of relaxation times is analyzed in [7] to diagnose the degradation mechanisms in the electrodes of the cell. Few specially selected frequencies are chosen to diagnose the battery SOH in [5], which indicates EIS could be possibly used in batteries' second-life applications. The authors in [11] use AC impedance to predict the overcharge and thermal runaway of the Li-ion battery.

Battery EIS measurement is performed in the range of kHz to mHz [12]–[14]. It is a time-consuming procedure for EIS measurement, especially in low frequency areas. Another requirement is that the battery itself should be kept in thermo-electrical equilibrium during the test period. Accordingly, only a small signal can be injected into the Li-ion battery for not

This work is financially supported by the Natural Science Foundation of China under Grant 52107229, and the Sichuan Science and Technology Program under Grant 2021YJ0063, and the Fund of Robot Technology Used for Special Environment Key Laboratory of Sichuan Province under Grant 20kfkt01, and the Open Research Fund of Jiangsu Collaborative Innovation Center for Smart Distribution Network under grant XTCX202005, and University-level Research Foundation of Nanjing Institute of Technology under grant YKJ2019114. (Corresponding author: Jinhao Meng).

Jichang Peng is with the Smart Grid Research Institute, Nanjing Institute of Technology, Nanjing 211167, China (e-mail: pengjichang@njit.edu.cn).

Jinhao Meng and Xinghao Du are with the college of Electrical Engineering, Sichuan University, Chengdu, China (e-mail: jinhao@scu.edu.cn, duxinghao@stu.scu.edu.cn).

Lei Cai is both with the Faculty of Computer Science and Engineering, Xi'an University of Technology, Xi'an 710048, China, and Shaanxi Key Laboratory for Network Computing and Security Technology, Xi'an 710048, China (e-mail: cailei@xaut.edu.cn).

Daniel-Ioan Stroe is with AAU Energy, Aalborg University, Aalborg 9220, Denmark (email: dis@energy.aau.dk).

triggering any significantly electrochemical reactions [15]. In [13], the authors measure the EIS of a 6.5Ah Li-ion battery with only 0.5A AC current amplitude for a frequency sweep from 10mHz to 5kHz. It can be concluded that EIS is a sensitive measurement, which is challenging to be implemented in BMS and applied online. Recently, some works [10], [12], [16]–[18] have managed to design a low cost prototype for a friendly EIS measurement in battery applications. An impedance-based BMS is designed to measure the impedance of a 50 Ah battery from 1 to 1000Hz [10]. Additionally, a low-complexity onboard impedance measurement system is proposed in [12] utilizing a high-power dual active bridge converter, which can measure the frequency in the range of 0.1-500 Hz. A MOSFET-based equalization circuit for the battery impedance measurement with a sinusoidal signal is proposed in [16]. A wireless charger is used to measure the battery impedance online in [18]. Besides hardware design, signal generation and processing also require more attention since more informative injection and accurate EIS calculation are always preferred in this case. More research is still needed to improve the efficiency as well as the accuracy of the EIS measurements.

To alleviate the above issues, great efforts have been made on developing the excitation signals with a series of frequency superposition and related data processing methods [19], [20]. Recently, multi-steps [21], multi-sines [22]–[25], and Pseudo Random Sequence (PRS) [8], [19], [26]–[28], *etc*. have been investigated for battery EIS measurement. Mutilsinusoidal signal in the ranges of 1-1.8 kHz has been chosen to obtain the battery impedance in [23], which is further used to estimate the battery capacity. A step signal is proposed in [21] to improve the measurement speed of the multi-sines method, and a 200 Hz step waveform is selected to test a 2.6 Ah 18650 Li-ion battery for validation. A random integer number white noise approximation is proposed in [28] to measure the impedance of the battery online, while the cross-correlation technique is used for signal generation. Among all the broadband signal generation methods, PRS has a similar statistical property to white noise and is easy to implement as explained in [19], [29].

According to the above description, it's clear that much effort has been made to generate the multi-frequencies signal for battery EIS measurement. However, the responses of those broadband signals are more difficult to be processed compared with single frequency injection. A powerful signal processing procedure should be designed to accurately extract the useful EIS measurement from the especially low Signal-to-Noise Ratio (SNR) signals. Most existing works still use the Moving Average Filter (MAF) [19], [28] to smooth the measured impedance. Large deviations may exist because of the limited ability of those linear filters, which inspires us to propose a novel impedance measurement method utilizing the power spectral density characteristics of the exciting signal.

This paper proposes a fast Li-ion battery impedance measurement method to extract the impedance spectra from the PRS signals. Considering that the synthetic signals composed of multi-frequencies can not receive high SNR responses at all broadband frequencies, we design a novel data cleaning procedure to extract the worthwhile information from the original measurement by integrating the real and imaginary parts, and PS into a three Dimensional (3D) cloud. The Power Spectrum (PS) reflects the power of a signal at various frequencies and can be regarded as a critical indicator to evaluate the effectiveness of the measured impedance. To the best of our knowledge, this is the first time to use a 3D cloud data cleaning method for improving the accuracy of the battery EIS measurement.

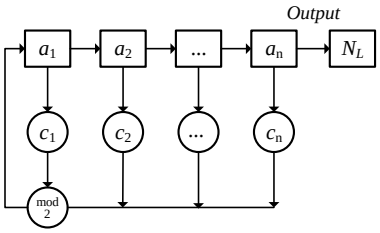

Fig. 1. The linear feedback shift registers for PRS generation

The main contributions of this paper lie in the following aspects:

1) A Nyquist plot-based 3D cloud is first reconstructed for the data cleaning of impedance measured by PRS, which utilizes the PS property of the injected signal.
2) A statistical based multiple selection mechanism is designed to remove the outliers and obtain a smooth battery EIS curve without any deformations.
3) The accuracy of our method is proven through the experimental tests on a 3000mAh Li-ion battery under different SOCs and temperatures.

This paper is organized into five sections. Section II introduces the implementation of the fast battery impedance measurement. The proposed data processing procedure is detailed in Section III. Experimental validation is illustrated in Section IV. Section V summarises the main conclusion of this work.

II. Fast Battery Impedance Measurement

PRS is used to measure the battery EIS in a short time. This section will briefly introduce the principle of PRS and its characteristics, and the battery impedance calculation method.

A. Pseudo Random Sequence

PRS can simulate the white noise in discrete time, and is a superior way to excite the battery at all frequencies in theory compared with other signals. The Maximum Length Binary Signal (MLBS) is one of the commonly used PRSs, which could be finalized by multi-stage linear feedback shift registers as shown in Fig. 1. Let us define N_L as the length of PRS, and the PRS can be generated by an *n*-th order shift registers as follows.

$$N_L = 2^n - 1 \tag{1}$$

Afterwards, a_n can be obtained by modulo 2 operation,

$$a_n = (\sum_{i=1}^{n} c_i a_i) \ mod \ (2) \tag{2}$$

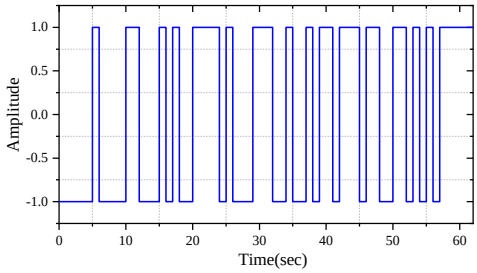

(a) Time domain

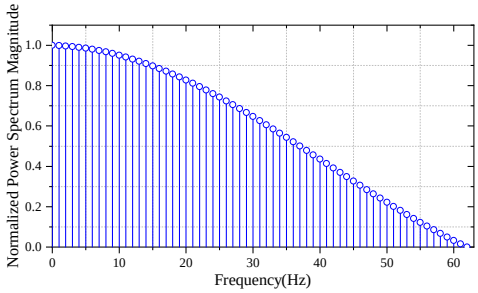

(b) Frequency domain

Fig. 2. An example of MLBS with N_L = 63 and f_c = 1Hz

where a_n has only two states 0 or 1 which indicate the binary sequence generates in GF(2).

The coefficients c_i can be calculated by a primitive polynomial according to the values of n and N_L. It is easy to understand the frequency resolution f_r of PRS should be,

$$f_r = f_c/N_L \tag{3}$$

where f_c is the clock frequency of the PRS.

A MLBS with N_L = 63 and f_c = 1Hz is illustrated in Fig. 2 to explain the feature of a typical PRS. The amplitudes of the MLBS toggle between level 1 and -1 as Fig. 2(a). The Root Mean Square (RMS) of the MLBS is 1. In the frequency domain, the power spectrum magnitude follows the $(sin^2x)/x^2$ envelope as illustrated in Fig. 2(b). It means that the PS of the MLBS gradually decays with increasing frequency. Additionally, the amplitude of the MLBS at f_n can be calculated as,

$$A_{MLBS}(f_n) = \frac{2a\sqrt{N_L+1}}{N_L}\frac{sin(\pi n/N_L)}{(\pi n/N_L)} \tag{4}$$

where f_n = $(n-1)f_r$.

When the $f_n = 1/3f_c$, the magnitude of MLBS rapidly decreases. Thus, N_L and f_c must be carefully designed for a specific application.

B. Battery Impedance Calculation

For the battery impedance measurement with PRS, the MLBS should be injected into the battery within the frequencies [f_{max}, f_{min}]. According to the property of MLBS, f_{min} has to be larger than f_r and f_{max} should be set to $0.4f_c$.

In the frequency range [f_{min}, f_{max}], the impedance can be calculated from the injected signal and the corresponding battery responses. Let's define the current $i(t)$ is injected into a Li-ion battery, and the voltage $v(t)$ is measured accordingly. Then, the Fourier transform of $i(t)$ and $v(t)$ can be obtained,

$$\begin{cases} V(k) = \sum_{k=0}^{N-1} v(t)e^{-j2\pi kt/N} \\ I(k) = \sum_{k=0}^{N-1} i(t)e^{-j2\pi kt/N} \end{cases} \tag{5}$$

From (5), the battery impedance at a specific frequency is calculated by,

$$\hat{Z}(k) = \frac{V(k)}{I(k)} \tag{6}$$

where $\hat{Z}(k)$ is the impedance of the k-th frequency.

The k-th frequency is kf_k, while the f_k is defined as,

$$f_k = f_s/N_s \tag{7}$$

where f_s is the sampling frequency, and N_s is the number of the sampling data.

III. The Proposed Data Processing Procedure

Although PRS can inject a broadband signal into the battery within a short period, impedance measurement through PRS suffers from noise and other interferences. Considering the fact that the signal with low PS is easily contaminated by noise and the PS of all the frequencies in Fig. 2 is not equally distributed, the PS property of PRS is utilized in this section for an accurate battery impedance measurement.

A. Power Spectrum

PS describes the distribution of the signal's power with frequency variation. Since white noise is a stationary process, the PS of a PRS can be described by its autocorrelation function according to Wiener-Khinchin theorem as follows,

$$S_{xx}(f) = \sum_{k=-\infty}^{+\infty} r_{xx}[k]e^{-j2\pi kf} \tag{8}$$

$$r_{xx}(f) = E[x[n]x[n-k]] \tag{9}$$

where S_{xx} is the power spectrum of $X[n]$.

Once the periodogram is used for the PS calculation, the MLBS can be regarded as a finite energy sequence. According to (4), the PS $P_{MLBS}(f_n)$ can be computed as,

$$P_{MLBS}(f_n) = \frac{(I_{MLBS}(f_n))^2}{f_n} \tag{10}$$

$$P_{MLBS\_n}(f_n) = \frac{(I_{MLBS}(f_n))^2}{f_n * P_{MLBS}(f_1)} \tag{11}$$

where $I_{MLBS}(f_n)$ is the amplitude of the MLBS at frequency f_n after Fourier transform.

It is easy to understand that there always exists a $P_{MLBS\_n}(f_n)$ for each f_n, which creates an opportunity to integrate the PS to the battery impedance. Once the PS is low, the signal is less informative with a lower possibility to be a valid value. Thus, PS can be regarded as a critical index to evaluate the signal at different frequencies.

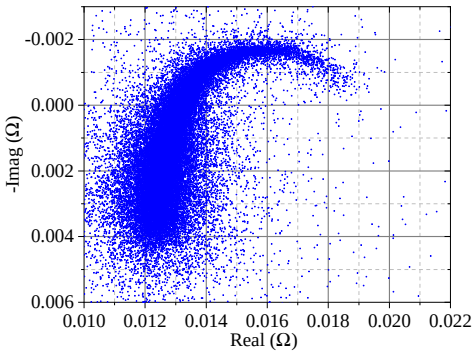

Fig. 3. The impedance of a Li-ion battery with MLBS

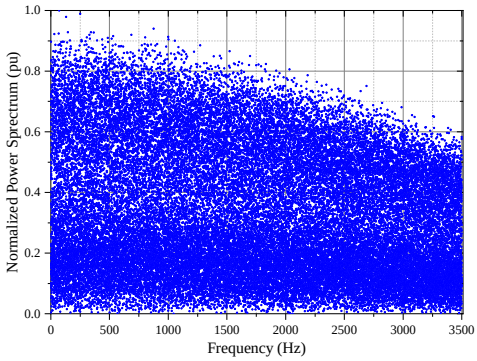

Fig. 4. The normalized power spectrum of a Li-ion battery with MLBS

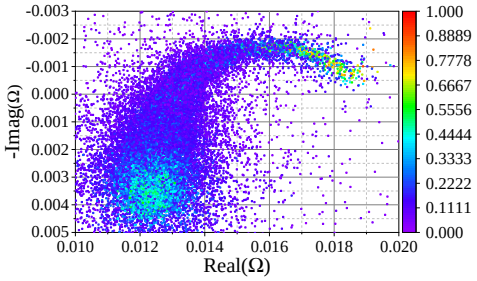

Fig. 5. The 3D cloud of Li-ion battery impedance

B. Reconstruction of the 3D Cloud

Li-ion battery should be treated as a linear system for the impedance measurement, and we will use the galvanostatic mode in this work. The following impedance in Fig. 3 can be obtained from a Li-ion battery when using MLBS. It is found from Fig. 3 that the high frequency area is contaminated by noise, and the shape of the normal impedance could only be seen in low frequency range. The main reason for such a phenomenon is the attenuation of the PS with the increasing frequency. Therefore, it is difficult to directly obtain useful impedances from the Nyquist curve in Fig. 3.

The $P_{MLBS\_n}(f_n)$ of the MLBS signal for the above battery impedance is shown in Fig. 4. We find that the PS of the MLBS gradually attenuates with the increase of the frequency. Also, it is clearly recognized that the PS fluctuates even between similar frequencies. Generally, a large PS signal means more power is injected into the battery, which has a higher chance against noise interference and then measures an accurate impedance. Then, besides the impedance value for specific frequencies, can be regarded as another property for the impedance measurement. Based on the above rules, we reconstruct the Nyquist plot of the battery impedance with PS information to form a 3D cloud in Fig. 5. In this way, the PS property is merged into the battery impedance measurement, which could be further used for data cleaning.

In Fig. 5, the colormap of the 3D cloud shows the intensity of the PS for each measured impedance. For example, the green and yellow dots have a higher PS than the blue ones. It is obvious from Fig. 5 that the blue dots deviate from the main data group, which are more likely to be outliers of the EIS measurement. In addition, the green color dots with high-intensity PS are centered in the middle of the dataset which is also consistent with the basic shape of the impedance spectrum. Massive scattered and disordered blue dots in Fig. 5 also prove the correctness of the above analysis. Therefore, by the reconstruction of a 3D cloud, the PS property can be used to process the impedance measurement of a Li-ion battery. Once the impedance with low-intensity PS is removed, accurate battery impedance measurements can be expected.

C. 3D Cloud Cleaning Method for Impedance Measurement

From the above analysis, it is possible to clean the impedance on the foundation of the reconstructed 3D cloud. Here, we propose a statistical based multiple selection mechanism to obtain the battery EIS.

As shown in Fig. 5, the density of the dots in the 3D cloud can be utilized to process the calculation results of the impedance. In order to evaluate the statistical characteristics of the impedance dots in Fig. 5, a neighbourhood area A is defined at first. The average Euclidean distance $\overline{d_k}$ of the k-th dot with coordinate (x_k, y_k, z_k) in A is then calculated as,

$$\overline{d_k} = (1/m) * \sum_{a=1}^{m} \sqrt{(x_k - x_a)^2 + (y_k - y_a)^2 + (z_k - z_a)^2} \tag{12}$$

where $(x_a, y_a, z_a) \in A$ and m is number of dots in area A.

The mean $\mathbb{E}[\overline{d_k}]$ and variance $\mathbb{E}[\overline{d_k}]$ of $\overline{d_k}$ can be obtained from (13) and (14),

$$\mathbb{E}[\overline{d_k}] = (1/N_k) * \sum_{k=1}^{n} \overline{d_k} \tag{13}$$

$$\Delta[d_k] = \sqrt{(1/N_k) * \sum_{k=1}^{N_k} (\overline{d_k} - \mathbb{E}[\overline{d_k}])^2} \tag{14}$$

where N_k is $m + 1$.

Afterwards, a reconstructed 3D cloud cleaning method is proposed in Algorithm 1 for automatically selecting the effective impedance values. Considering the natural diversity of the impedance in the high and low frequency region of the

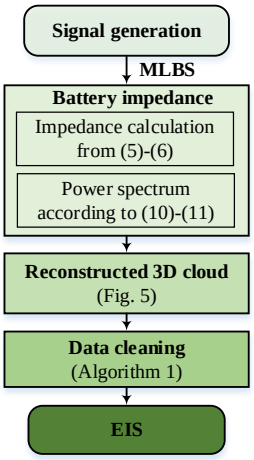

Fig. 6. The diagram of the proposed fast battery impedance measurement

3D cloud, all the measurements are divided into N_g groups for the convenience of data cleaning. In each group, a threshold Γ_{th} is calculated from the step 3 of Algorithm 1, where N_{th} is a coefficient tuning the threshold Γ_{th}. Then, the cleaning step can utilize Γ_{th} to decide which dot should be removed from the 3D cloud. After receiving the flag $Imp_{flag,k}$ from Algorithm 1, the battery EIS $\hat{Z}_{EIS}(k)$ can be obtained through the following operation,

$$\hat{Z}_{EIS}(k) = \hat{Z}(k) * Imp_{flag,k} \tag{15}$$

Algorithm 1 Reconstructed 3D Cloud Cleaning

Input: $\mathbb{E}[\overline{d_k}]$, $\Delta[d_k]$, A

Initialization: Divide the impedance values into N_g groups
for $i \leftarrow 1$ to N_g **do**
  $\Gamma_{th} \leftarrow \mathbb{E}[\overline{d_k}] + N_{th} * \Delta[d_k]$ //Calculate the threshold
  for $j \leftarrow 1$ to m **do**
    $\overline{d_k}$ calculation //From (12)
    if $\overline{d_k} < \Gamma_{th}$ **then**
      $Imp_{flag,k} \leftarrow 1$
    else
      $Imp_{flag,k} \leftarrow 0$
    end if
  end for
end for
return Imp_{flag}

Then, it is possible to fast and accurately obtain the Li-ion battery EIS through the above well-designed procedures in Fig. 6. The MLBS signal is generated for battery impedance measurement at first, and then the impedance and its PS are calculated in the frequency domain. Afterwards, a 3D cloud is reconstructed by integrating the impedance with its PS property. According to a statistical based multiple selection mechanism, the effective impedance could be kept as the final results.

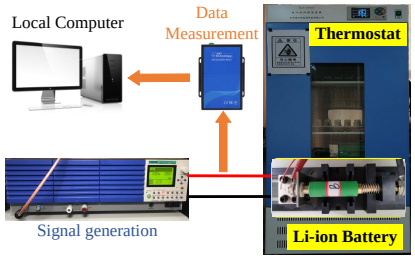

Fig. 7. The test bench for experimental validation

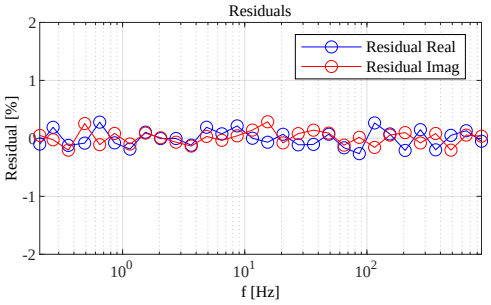

Fig. 8. The Kramers-Kronig test of the reference

IV. Experimental Validation

A. Experimental Test Bench

In this section, we validate the proposed method using the test bench shown in Fig. 7. A bi-directional power source is chosen to provide the injected signals for the Li-ion battery, a data acquisition board is used to obtain all the voltage and current measurements. A 18650 NMC based Li-ion battery, with a capacity of 3000mAh and a voltage range between 2.0V and 4.25V, is chosen to verify the proposed method. The battery is placed in a temperature chamber to control the ambient temperature during the test. In this work, the impedance is measured within the frequency range between 0.21Hz and 3.5kHz, which is enough to show the impedance shape of the chosen 18650 Li-ion battery. All the Li-ion battery impedance in this work are measured using the setup presented by Fig. 7. The reference EIS in this work is obtained by injecting only one frequency each time to the battery. The Kramers-Kronig relations are tested at first to prove the reliability and accuracy of the reference. As shown in Fig. 8, the residuals of the reference values are quite small, which indicates the measured reference is effective to be used for the experimental validation.

B. Validation of the 3D Cloud Cleaning

Following the steps in Algorithm 1, the number of dots in the nearest area m is defined as 100. Then, the 3D cloud in Fig. 5 is transferred to Fig. 9. By comparing the 3D cloud in those two figures, we find that those obvious outliers are removed from the dataset if only using the 3D cloud cleaning method one time. The contour of the EIS curve can be recognized from the dots in Fig. 9. When the impedance dots in the 3D cloud are converted to the Nyquist plot in Fig. 10, the result

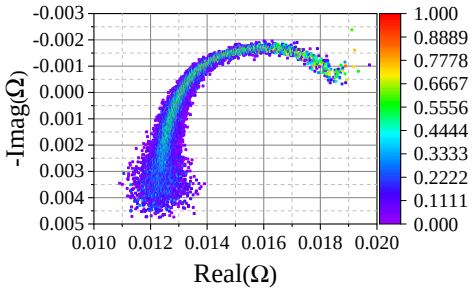

Fig. 9. 3D cloud cleaning with Algorithm 1

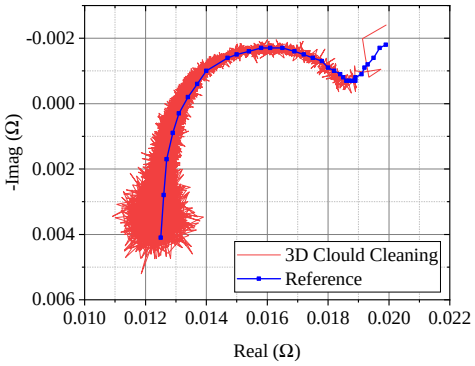

Fig. 10. 3D cloud cleaning results in Nyquist plot with N_g=1

from one-time 3D cloud cleaning is not satisfactory. The red curve around the reference values reflects that there is still too much useless impedance information left.

In order to clean the data with higher efficiency, the 3D cloud is divided into groups in line with the frequency range characteristics. Considering that the PS has a good linear relationship with frequency variation in logarithmic coordinates, those dots in the 3D cloud can be briefly grouped into three frequency regions at [0.21Hz, 10Hz], [10Hz, 1kHz], and [1kHz, 3.5kHz]. Thus, it forms three groups based on the frequency regions above, and N_g in Algorithm 1 will be 3 in the following experiments. The division of the frequency ranges can follow the distribution of the impedance measurement in a 3D cloud, especially, the number of the measurements and their PS characteristics should be fully considered. In this way, the characteristics of PS in the low, moderate, and high frequency areas can be fully utilized.

The results for 3D cloud cleaning with N_g=3 are shown in Fig. 11 that only 102 useful points are left, which indicates that the noise data is effectively removed after the 3D cloud cleaning procedure. The battery impedance values in Fig. 11 can be easily processed by data smooth filters such as Savitzky-Golay filter. Since the data smooth after 3D cloud cleaning is not difficult, other filters could also be used here.

C. Validation on EIS measurement

This section validates the EIS measurement of the proposed method. MAF is chosen to deal with the battery impedance measurements in [19], [30] when PRS is used. Thus, MAF is selected as a comparison method in this work. The expression of MAF is as follows,

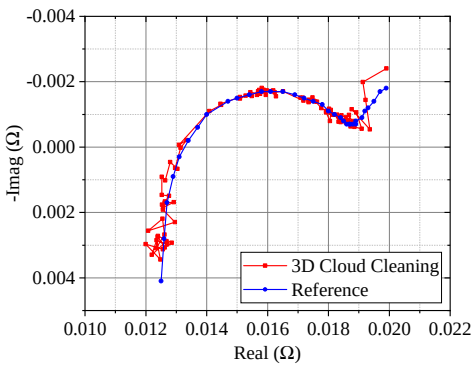

Fig. 11. 3D cloud cleaning with N_g=3

$$Z_{MAF}(i) = \frac{1}{M_w}\sum_{k=i}^{M_w} Z(i+k) \tag{16}$$

where M_w is the size of the moving window.

The EIS measurement results of the 18650 Li-ion battery under different SOCs are shown in Fig. 12. For SOC=20%, the proposed method is clearly close to the reference compared with the MAF method as illustrated in Fig. 12(a). Although there exist some offsets in the low frequency area, no outliers are identified in the impedance spectra presented in Figs. 12(b)-(c) for the proposed method. Meanwhile, the MAF method shows a larger error, and several outliers exist in the middle or high frequency area.

In order to quantitative analysis of the accuracy of EIS measurement for different methods, the Mean Absolute Percentage Error (MAPE) and the Normalized Root Mean Square Error (NRMSE) are calculated as follows,

$$MAPE = \frac{1}{M}\sum_{i=1}^{M}|1 - \frac{Z_m(i)}{Z_r(i)}| \tag{17}$$

$$NRMSE = \sqrt{\frac{1}{M}\sum_{i=1}^{M}(1 - \frac{Z_m(i)}{Z_r(i)})^2} \tag{18}$$

where M is the number of the measurement, Z_m and Z_r are the measured impedance and the corresponding reference respectively.

According to (16) and (17), the MAPE and NRMSE are listed in the TABLE. I. The average MAPE of the proposed method is 0.89%, while it is 1.62% for MAF. As for NRMSE, the proposed method is less than 33 % of the average NRMSE of MAF. Thus, both the MAPE and NRMSE of the proposed method are less than that of MAF, which proves the good accuracy of the proposed method.

For further verifying the performance of the proposed method under temperature variations, the test ambient temperature is controlled to 15^oC and 35 ^oC, and the Li-ion battery SOC is kept to 50%. The EIS measurement results of 15^oC are shown in Fig. 13. We find that large errors exist for MAF method in the middle frequency range. The proposed method still performs better than MAF in the whole frequency range. The MAPE and NRMSE of the results in 15^oC and 35 ^oC

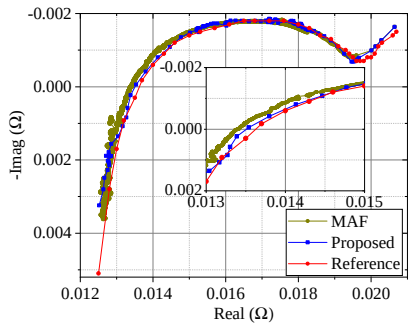

(a) SOC=20%

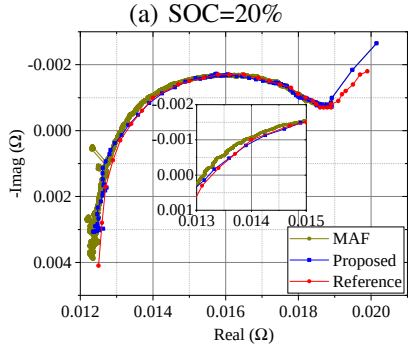

(b) SOC=50%

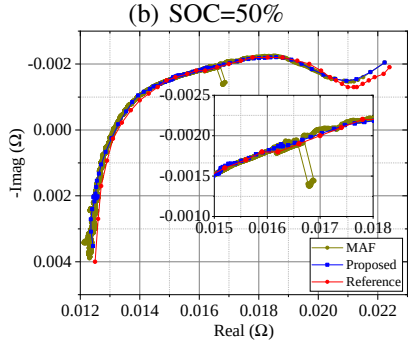

(c) SOC=80%

Fig. 12. A comparison of the EIS measurement results at T=25^oC

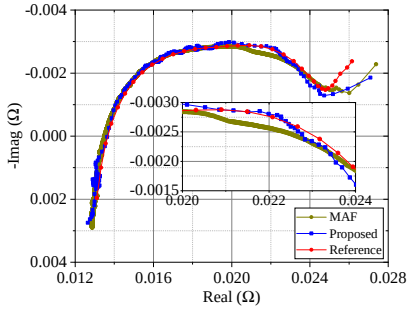

Fig. 13. EIS measurement results for SOC=50%, T=15^oC

are shown in the TABLE. II. It is noted that the accuracy of the proposed method has also been confirmed by a series of repeated tests. Based on the above validations, the superior performance of the proposed method can be confirmed.

V. Conclusion

This paper utilizes the PS property of the injected MLBS signal to reconstruct a 3D cloud for fast Li-ion battery impedance measurement. By creating a statistical based multiple selection mechanism for data cleaning, the massive impedance data can be effectively extracted from the original measurement. According to the PS characteristics in the different frequency ranges, the originally measured impedance is divided into 3 groups for 3D cloud data cleaning with higher efficiency. In this way, the proposed method can help measure the battery EIS accurately with MLBS in a short period.

The proposed method is validated on a 3000mAh Li-ion battery under various SOCs (20%, 50%, 80%) and temperatures (15^oC, 25^oC, 35^oC). The MAPE and NRMSE of the proposed method are much lower than the commonly used MAF method. The average MAPE of the proposed method is around 55% of MAF, and the average NRMSE of the proposed method is less than 33% of MAF for different SOCs. The advantages of the proposed method are thus proved through experimental validation. It is noted the proposed method can help the onboard EIS measurement with low-cost hardware, which is critical for improving the capability of BMS.

Future work will be to develop advanced PRS signals for a more efficient and accurate battery EIS measurement.

TABLE I
MAPE and NRMSE of Experimental Results at Different SOCs

Methods	Error	SOC=80%	SOC=50%	SOC=20%
MAF	MAPE	2.23%	1.32 %	1.30%
	NRMSE	1.83%	1.03 %	0.82%
Proposed	MAPE	1.04%	0.90 %	0.74%
	NRMSE	0.12%	0.49 %	0.60%

TABLE II
MAPE and NRMSE of Experimental Results at Different Temperatures

Methods	Error	T=15^oC	T=25^oC	T=35^oC
MAF	MAPE	2.92%	1.32 %	2.52%
	NRMSE	2.60%	1.03 %	2.05%
Proposed	MAPE	1.69%	0.90 %	2.39%
	NRMSE	0.64%	0.49 %	1.37%

References

[1] "EV-Volumes - The Electric Vehicle World Sales Database." [Online]. Available: https://www.ev-volumes.com/country/total-world-plug-in-vehicle-volumes/

[2] Q. Lin, J. Wang, R. Xiong, W. Shen, and H. He, "Towards a smarter battery management system: A critical review on optimal charging methods of lithium ion batteries," *Energy*, vol. 183, DOI https://doi.org/10.1016/j.energy.2019.06.128, pp. 220–234, 2019.

[3] M. Messing, T. Shoa, and S. Habibi, "Estimating battery state of health using electrochemical impedance spectroscopy and the relaxation effect," *Journal of Energy Storage*, vol. 43, DOI https://doi.org/10.1016/j.est.2021.103210, p. 103210, 2021.

[4] I. Babaeiyazdi, A. Rezaei-Zare, and S. Shokrzadeh, "State of charge prediction of EV Li-ion batteries using EIS: A machine learning approach," *Energy*, vol. 223, DOI https://doi.org/10.1016/j.energy.2021.120116, p. 120116, 2021.

[5] E. Locorotondo, V. Cultrera, L. Pugi, L. Berzi, M. Pierini, and G. Lutzemberger, "Development of a battery real-time state of health diagnosis based on fast impedance measurements," *Journal of Energy Storage*, vol. 38, DOI https://doi.org/10.1016/j.est.2021.102566, p. 102566, 2021.

[6] Y. Zhang, Q. Tang, Y. Zhang, J. Wang, U. Stimming, and A. A. Lee, "Identifying degradation patterns of lithium ion batteries from impedance spectroscopy using machine learning," *Nature Communications*, vol. 11, DOI 10.1038/s41467-020-15235-7, no. 1, p. 1706, 2020.

[7] J. Zhu, M. Knapp, X. Liu, P. Yan, H. Dai, X. Wei, and H. Ehrenberg, "Low-Temperature Separating Lithium-Ion Battery Interfacial Polarization Based on Distribution of Relaxation Times (DRT) of Impedance," *IEEE Transactions on Transportation Electrification*, vol. 7, DOI 10.1109/TTE.2020.3028475, no. 2, pp. 410–421, 2021.

[8] X. Du, J. Meng, J. Peng, Y. Zhang, T. Liu, and R. Teodorescu, "Sensorless Temperature Estimation of Lithium-ion Battery based on Broadband Impedance Measurements," *IEEE Transactions on Power Electronics*, 2022.

[9] A. A. Hussein and A. A. Fardoun, "An Adaptive Sensorless Measurement Technique for Internal Temperature of Li-Ion Batteries Using Impedance Phase Spectroscopy," *IEEE Transactions on Industry Applications*, vol. 56, DOI 10.1109/TIA.2020.2979783, no. 3, pp. 3043–3051, 2020.

[10] B. G. Carkhuff, P. A. Demirev, and R. Srinivasan, "Impedance-Based Battery Management System for Safety Monitoring of Lithium-Ion Batteries," *IEEE Transactions on Industrial Electronics*, vol. 65, DOI 10.1109/TIE.2017.2786199, no. 8, pp. 6497–6504, 2018.

[11] N. Lyu, Y. Jin, R. Xiong, S. Miao, and J. Gao, "Real-Time Overcharge Warning and Early Thermal Runaway Prediction of Li-Ion Battery by Online Impedance Measurement," *IEEE Transactions on Industrial Electronics*, vol. 69, DOI 10.1109/TIE.2021.3062267, no. 2, pp. 1929–1936, 2022.

[12] X. Wang, X. Wei, Q. Chen, and H. Dai, "A Novel System for Measuring Alternating Current Impedance Spectra of Series-Connected Lithium-Ion Batteries With a High-Power Dual Active Bridge Converter and Distributed Sampling Units," *IEEE Transactions on Industrial Electronics*, vol. 68, DOI 10.1109/TIE.2020.3001841, no. 8, pp. 7380–7390, 2021.

[13] D. Andre, M. Meiler, K. Steiner, C. Wimmer, T. Soczka-Guth, and D. U. Sauer, "Characterization of high-power lithium-ion batteries by electrochemical impedance spectroscopy. I. Experimental investigation," *Journal of Power Sources*, vol. 196, DOI https://doi.org/10.1016/j.jpowsour.2010.12.102, no. 12, pp. 5334–5341, 2011.

[14] D. I. Stroe, M. Swierczynski, A. I. Stan, V. Knap, R. Teodorescu, and S. J. Andreasen, "Diagnosis of lithium-ion batteries state-of-health based on electrochemical impedance spectroscopy technique," in *2014 IEEE Energy Conversion Congress and Exposition (ECCE)*, DOI 10.1109/ECCE.2014.6954027, pp. 4576–4582. IEEE, Sep. 2014.

[15] A. Lasia, "Electrochemical Impedance Spectroscopy and its Applications BT - Modern Aspects of Electrochemistry," B. E. Conway, J. O. Bockris, and R. E. White, Eds., pp. 143–248. Boston, MA: Springer US, 2002.

[16] M. Koseoglou, E. Tsioumas, D. Papagiannis, N. Jabbour, and C. Mademlis, "A Novel On-Board Electrochemical Impedance Spectroscopy System for Real-Time Battery Impedance Estimation," *IEEE Transactions on Power Electronics*, vol. 36, DOI 10.1109/TPEL.2021.3063506, no. 9, pp. 10 776–10 787, 2021.

[17] S. M. R. Islam and S. Park, "Precise Online Electrochemical Impedance Spectroscopy Strategies for Li-Ion Batteries," *IEEE Transactions on Industry Applications*, vol. 56, DOI 10.1109/TIA.2019.2958555, no. 2, pp. 1661–1669, 2020.

[18] E. Locorotondo, F. Corti, L. Pugi, L. Berzi, A. Reatti, and G. Lutzemberger, "Design of a wireless charging system for online battery spectroscopy," *Energies*, vol. 14, DOI 10.3390/en14010218, no. 1, 2021.

[19] J. Sihvo, D. I. Stroe, T. Messo, and T. Roinila, "Fast Approach for Battery Impedance Identification Using Pseudo-Random Sequence Signals," *IEEE Transactions on Power Electronics*, vol. 35, DOI 10.1109/TPEL.2019.2924286, no. 3, pp. 2548–2557, 2020.

[20] A. Waligo and P. Barendse, "A comparison of the different broadband impedance measurement techniques for lithium-ion batteries," in *2016 IEEE Energy Conversion Congress and Exposition (ECCE)*, DOI 10.1109/ECCE.2016.7854661, pp. 1–7, 2016.

[21] J. A. Qahouq and Z. Xia, "Single-Perturbation-Cycle Online Battery Impedance Spectrum Measurement Method with Closed-Loop Control of Power Converter," *IEEE Transactions on Industrial Electronics*, vol. 64, DOI 10.1109/TIE.2017.2686324, no. 9, pp. 7019–7029, 2017.

[22] D. A. Howey, P. D. Mitcheson, V. Yufit, G. J. Offer, and N. P. Brandon, "Online Measurement of Battery Impedance Using Motor Controller Excitation," *IEEE Transactions on Vehicular Technology*, vol. 63, DOI 10.1109/TVT.2013.2293597, no. 6, pp. 2557–2566, 2014.

[23] Z. Xia and J. A. A. Qahouq, "State-of-Charge Balancing of Lithium-Ion Batteries With State-of-Health Awareness Capability," *IEEE Transactions on Industry Applications*, vol. 57, DOI 10.1109/TIA.2020.3029755, no. 1, pp. 673–684, 2021.

[24] W. Huang and J. A. Qahouq, "An online battery impedance measurement method using DC-DC power converter control," *IEEE Transactions on Industrial Electronics*, vol. 61, DOI 10.1109/TIE.2014.2311389, no. 11, pp. 5987–5995, 2014.

[25] S. H. Kim, H. M. Lee, and Y. J. Shin, "Aging Monitoring Method for Lithium-Ion Batteries Using Harmonic Analysis," *IEEE Transactions on Instrumentation and Measurement*, vol. 70, DOI 10.1109/TIM.2020.3043097, pp. 1–11, 2021.

[26] G. Nusev, Juričić, M. Gaberšček, J. Moškon, and P. Boškoski, "Fast Impedance Measurement of Li-Ion Battery Using Discrete Random Binary Excitation and Wavelet Transform," *IEEE Access*, vol. 9, DOI 10.1109/ACCESS.2021.3058368, pp. 46 152–46 165, 2021.

[27] Z. Geng, T. Thiringer, Y. Olofsson, J. Groot, and M. West, "On-board Impedance Diagnostics Method of Li-ion Traction Batteries Using Pseudo-Random Binary Sequences," in *2018 20th European Conference on Power Electronics and Applications (EPE'18 ECCE Europe)*, pp. P.1–P.9, 2018.

[28] T. N. Gücin and L. Ovacik, "Online Impedance Measurement of Batteries Using the Cross-Correlation Technique," *IEEE Transactions on Power Electronics*, vol. 35, DOI 10.1109/TPEL.2019.2939269, no. 4, pp. 4365–4375, 2020.

[29] A. J. Fairweather, M. P. Foster, and D. A. Stone, "Battery parameter identification with Pseudo Random Binary Sequence excitation (PRBS)," *Journal of Power Sources*, vol. 196, DOI https://doi.org/10.1016/j.jpowsour.2011.06.072, no. 22, pp. 9398–9406, 2011.

[30] J. Sihvo, T. Roinila, and D.-I. Stroe, "Novel fitting algorithm for parametrization of equivalent circuit model of li-ion battery from broadband impedance measurements," *IEEE Transactions on Industrial Electronics*, vol. 68, DOI 10.1109/TIE.2020.2988235, no. 6, pp. 4916–4926, 2021.

Jichang Peng received the B.S. degree in electrical engineering from the North China University of Water Resources and Electric Power, Zhengzhou, China, in 2010, and the M.S. degree in control theory and control engineering and the Ph.D. degree in electrical engineering from Northwestern Polytechnical University, Xi'an, China, in 2013 and 2019, respectively.

He is currently a Lecturer in Nanjing Institute of Technology, Nanjing, China. His research interests include battery modeling, energy management, and aircraft starter/generator and sensorless control of brushless synchronous machines.

Jinhao Meng (M'19) received the M.S. degree in control theory and control engineering and the Ph.D. degree in electrical engineering from the Northwestern Polytechnical University (NPU), Xi'an, China, in 2013 and 2019, respectively. He was supported by the China Scholarship Council, as a Joint Ph.D. student with the Department of Energy Technology, Aalborg University, Aalborg, Denmark. He is currently an Associate Professor in Sichuan University, Chengdu, China.

His research interests include battery modeling, battery states estimation, and energy management of battery energy storage systems.

Xinghao Du received the B.S. degree in electrical engineering from Civil Aviation Flight University of China, Deyang, China, in 2020. He is currently working toward the M.S. degree in electrical engineering with the College of Electrical Engineering, Sichuan University, Chengdu, China.

His current research interests include lithium-ion battery modeling, states estimation, and broadband impedance measurements.

Lei Cai received the Ph.D degree from Northwestern Polytechnical University (NPU), Xi'an, China, in 2017. He was supported by the China Scholarship Council as a joint Ph.D. student with the School of Computer Science, University of Birmingham, Birmingham, U.K. He is currently a lecturer with the Faculty of Computer Science and Engineering, Xi'an University of Technology, Xi'an, China.

His current research interests include evolutionary computation, optimization, data-driven battery modeling, battery states estimation, and energy management.

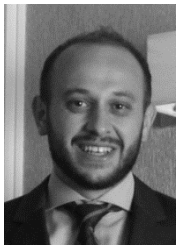

Daniel-Ioan Stroe (M'14) received the Dipl.-Ing. degree in automatics from "Transilvania" University of Brasov, Romania, in 2008, and M.Sc. degree in wind power systems from Aalborg University, Aalborg, Denmark, in 2010. He has been with AAU Energy, Aalborg University since 2010, from where he obtained his Ph.D. degree in lifetime modeling of Lithium-ion batteries in 2014.

He is currently an Associate Professor with AAU Energy and the leader of the Batteries research group. He was a Visiting Researcher with RWTH Aachen, Germany, in 2013. He has co-authored one book and over 170 scientific peer-review publications most of them on topics related to Lithium-ion battery performance and lifetime modeling and battery state estimation. Furthermore, he is serving as a special issue editor and topic editor for various journals. Daniel's current research interests are in the area of energy storage systems for grid and e-mobility, Lithium-based batteries' testing, modeling, lifetime estimation, and their diagnostics.